# Persistent photoconductivity and two-band effects in GaAs/$Al_xGa_{1-x}As$ heterojunctions

R. Fletcher and E. Zaremba
*Department of Physics, Queen's University at Kingston, Kingston, Ontario, Canada K7L 3N6*

M. D'Iorio
*Division of Physics, National Research Council of Canada, Ottawa, Canada K1A 0R6*

C. T. Foxon and J. J. Harris
*Philips Research Laboratories, Redhill, Surrey, RH1 5HA, England*
(Received 26 September 1989; revised manuscript received 12 January 1990)

We have measured the mobility and individual subband electron densities of GaAs/$Al_xGa_{1-x}As$ heterojunctions (with $x \simeq 0.33$) exhibiting two subband occupancy as a function of total two-dimensional electron-gas density. The density is varied by means of persistent photoconductivity using either red or infrared radiation. The latter is filtered to prevent electron-hole–pair excitations in the GaAs. Different behavior is observed in the two cases which can be attributed to differing excitation mechanisms. Infrared radiation leads to ionization of *DX* centers in the $Al_xGa_{1-x}As$ while red radiation preferentially leads to the excitation of electron-hole pairs in the GaAs. This latter process continues until the acceptor depletion layer is exhausted, at which point *DX* excitations take over. Detailed calculations (with no adjustable parameters) of the electronic structure provide a good account of the observed electron areal densities in the two subbands as a function of total density for both types of illumination. The mobility is calculated with use of an estimate of the ionized-impurity charge distribution based on a model in which the Si donors in the $Al_xGa_{1-x}As$ have both a shallow and a deep level. The general trends of the theoretical results are in good agreement with those of the experimental data, but the calculated mobility tends to be too low in absolute magnitude. The calculations indicate that complete ionization of all donors in the $Al_xGa_{1-x}As$ at saturation is incompatible with the observed density dependence of the mobility. The theoretical results also show that the relative magnitudes of the transport and quantum lifetimes for electrons in the two subbands depend sensitively on the illumination conditions. For example, the second-subband transport lifetime can be roughly a factor of 2 greater (red) or smaller (ir) than that of the first subband.

## I. INTRODUCTION

The main purpose of this work is to extend previous studies on persistent photoconductivity (PPC) in semiconductor heterojunctions and, in particular, to study the effects of using photon energies $\nu$ in the two regimes $h\nu < E_g$ (infrared) and $h\nu > E_g$ (red) where $E_g$ is the energy gap of the GaAs in the junction.[1–4] With infrared (ir) radiation, the main effect is believed to be the excitation of the so called *DX* centers[5–11] in the $Al_xGa_{1-x}As$ to produce electrons; the electrons are, at least in part, added to the two-dimensional electron gas (2D EG) at the interface leaving positively charged donors in the $Al_xGa_{1-x}As$. With red light this process can still occur. However, the radiation can also be absorbed through the production of electron-hole (*e-h*) pairs in the GaAs, either in the cap layer or in the layer forming the junction. In the latter case the pair is separated by the junction electric field with the electron going to the 2D EG and the hole neutralizing a negatively ionized acceptor in the GaAs depletion layer. The two mechanisms, i.e., *DX*-center ionization and *e-h*–pair generation, have different effects on the electrostatic potential in the interface region and this, in turn, causes different variations in the wave functions of the electrons in the 2D EG.

Ando[12] and Stern and Das Sarma[13] have theoretically studied the effects on the electronic energy levels of changing the 2D EG density $n_T$ (where the subscript refers to the total density to distinguish it from the individual subband occupancies) and changing the total areal depletion charge density $n_a$ in the GaAs. They find that the energy separation, $E_{10}$, of the first two subbands increases with both $n_T$ and $n_a$, with the latter being a very strong effect. In the present experiments we can increase $n_T$, leaving $n_a$ unchanged, by using ir radiation, or we can decrease $n_a$ (with an equivalent increase in $n_T$) by using red light. By measuring the occupations of the first and second subbands we have a sensitive probe of the subband energy levels and their dependence on illumination conditions. In the present experiments the subband occupancies have been obtained with high resolution and the observed behavior as a function of illumination is well described by the aforementioned excitation mechanisms. In addition, the interpretation of the data was checked by performing self-consistent electronic structure calculations which required, as input, values of $n_T$ and $n_a$. In a

 

previous paper[1] the latter was inferred from a comparison of the observed subband density behavior with the results of such electronic structure calculations.[12,13] However, in this paper we have an independent method to determine $n_a$ which enables the calculations to be performed for the specific samples studied with no adjustable parameters. The resulting good agreement between calculations and experiment not only corroborates the proposed excitation mechanisms but also attests to the accuracy of electronic structure calculations when carried out for well-characterized heterojunctions.

The transport mobility also provides information about the electronic structure through the onset of intersubband scattering. The observed density dependence of mobility correlates well with the illumination data. In addition, the mobility provides information regarding the spatial distribution of ionized impurities throughout the system, and in particular in the heavily doped $Al_xGa_{1-x}As$ layer. In principle this distribution can be monitored as a function of illumination via transport properties, thereby clarifying the mechanisms of charge generation and loss. In this work we have made an attempt to analyze our data with this objective in mind, but at present a fully consistent picture has yet to be achieved.

The main uncertainty in the calculations of mobility stems from the incomplete knowledge of the ionized impurity distribution. We have assumed a reasonable starting point before illumination to be one of thermodynamic equilibrium in which the charge state of a donor is dictated by the position of the donor level relative to a common chemical potential. Previous work[5–9] has demonstrated the existence of both shallow and deep donors, the latter identified as the *DX* centers, and both species were included in our model. By adjusting the depth of the deep donor level and the ratio of deep to shallow donors, we find that electrostatically consistent distributions are possible only for certain ranges of these parameters. Once the distributions have been specified, the impurity-induced scattering probabilities can be calculated and the mobility evaluated.

In this model the neutral *DX* center are the source of PPC. During illumination the photoionized *DX* centers provide additional electronic scattering but the results indicate that only a small fraction of the originally neutral *DX* centers can be ionized, otherwise the final mobility would be much lower than that observed. If we simply assume that the number of scattering centers changes little during illumination, the calculated and observed mobilities show very similar behavior as a function of 2D EG density. Although we cannot offer a definite explanation for why this assumption is reasonable, the good correlation between theory and experiment does suggest that the assumed ionized-impurity distributions are indeed representative of the actual conditions in the heterojunctions.

In the course of the mobility calculations we have also evaluated the transport and quantum lifetimes of both subbands. These results show that the type of illumination has a strong effect, particularly on the upper subband lifetimes which behave in completely different ways in the two cases. In an earlier paper[14] we presented some data of the subband quantum lifetimes as determined by measurements of the Dingle temperatures. Although we do not present such data in the present paper, the general features of the experimental results on the mobility are in accord with the theoretical predictions of the various lifetimes and the discussion of them given previously.[14]

The rest of the paper is arranged as follows. In Sec. II we describe our experimental techniques, and present our experimental results in Sec. III, along with brief interpretations of the important features. Section IV is devoted to a detailed discussion of the theoretical aspects related to the experiments, of the assumptions required in the calculations, and of the comparison of the calculated results with experiment.

## II. EXPERIMENTS

Most of the experiments were performed at a temperature in the range 1.2–1.4 K but on one occasion to be mentioned later, limited data were obtained at 77 K. The sample was located in a vacuum tight can with He exchange gas providing a thermal link to the liquid $^4$He. Detailed results were obtained for three samples (see Table I) chosen because in the dark only the first subband is populated, but when illuminated a second subband becomes occupied. Two of the samples were from the same wafer [labeled No. 1 (G130A) and No. 2 (G130B)]. We have previously published some data from sample No. 1,[14] and No. 3 (G131) is from the same wafer as a sample investigated by Harris *et al.*[1] The general behavior of all the samples is similar.

Two light emitting diodes (LED's), about 25 mm from the sample, provided the radiation. The red LED has a peak emission at 665 nm and the ir LED peaks at 935 nm; both numbers are appropriate at room temperature and will move to shorter wavelengths at low temperature. To completely eliminate photons with $h\nu > E_g$, the ir diode was used with a filter. It was found that a ten-period GaAs/GaAlAs superlattice provided adequate filtering in the sense that there was no evidence of $e$-$h$-pair excitations. This was confirmed in later experiments which used bulk InP (with a band gap of about 0.1 eV less than bulk GaAs) as a filter; no difference was observed between this and the superlattice. In contrast, bulk GaAs was found to be an unsuitable filter since $e$-$h$-pair generation in the GaAs of the heterojunction was still observed to occur. Either the band gap of the bulk material is slightly larger than that appropriate to the junction, which permits some radiation above the band gap to be transmitted, or radiation just above the gap is not attenuated sufficiently. Nevertheless the amount transmitted is only a small fraction of the total and so provided an interesting case in which the observed behavior is intermediate to that found with either red or ir illumination. This is discussed in more detail later.

The diodes were activated by current pulses of known duration. After each illumination, various data were taken beginning with the zero-field resistivity. To obtain the total carrier density $n_T$, the Hall resistivity $\rho_{yx}$ was measured at about 100 points, typically over the range of 0.15–0.95 T for sample 3 and somewhat higher for sam-

ple 1. The lower limit satisfied $\omega\tau^t > 1$ (with $\omega$ the cyclotron frequency and $\tau^t$ the transport relaxation time) so we expect $\rho_{yx} = B/n_T e$. At the upper limit the quantum oscillations in $\rho_{yx}$ are becoming large enough to affect the quality of the straight line fits to the data. We also monitored the de Haas–Shubnikov (dHS) oscillations, typically over the range of 0.7–1.5 T for sample 3, to determine the number of carriers in each band. In this paper we always quote $n_T$ as derived from $\rho_{yx}$ data, $n_0$ (the lower subband density) from dHS data, and $n_1$ from $n_T - n_0$. Our data on $n_1$ as derived from dHS oscillations (when there are enough oscillations to make this practical) are in reasonable agreement with $n_T - n_0$ (typically $\pm < 0.1 \times 10^{15}$ $m^{-2}$) but show much more scatter. It might also be noted that the high-field condition on $\rho_{yx}$, i.e., $\omega_c \tau^t > 1$, is appropriate to the average transport relaxation time $\langle \tau^t \rangle$ when both bands are occupied, and this is dominated by the lower subband relaxation time $\tau_0^t$ for our samples. If the upper subband electrons have a significantly different relaxation time $\tau_1^t$, in particular much shorter than $\tau_0^t$, one might question whether $n_T - n_0$ as obtained above is a good measure of $n_1$. We have investigated this point within the two-band model of Wilson.[15] We did this by generating $\rho_{yx}$ data for various $\tau_1^t/\tau_0^t$ and analyzing it exactly as for the experimental data, i.e., assuming the slope gives $1/n_T e$. We find that for $0.2 < \tau_1^t/\tau_0^t < 10$ we obtain $n_1$ accurate to $\leq 5\%$ by this procedure (assuming $n_0$ is known), though for $\tau_1^t/\tau_0^t < 0.2$ the error in $n_1$ rapidly increases. These checks suggest that the adopted procedure should be generally reliable.

It should also be noted that the measurements on each sample were obtained with a number of cooldowns. Since some variability with cooldown of the starting parameters, e.g., mobility and $n_T$, was observed we have presented data obtained on a single cooldown where possible so that a consistent correlation of different parameters can be made. This is obviously not possible for data taken with red and ir illumination which require successive warming and cooling and it will be noticed that in these cases the starting points on some of the graphs are not exactly the same.

## III. EXPERIMENTAL RESULTS

Figure 1(a) shows the total carrier density $n_T$ in samples 1 and 3 as a function of integrated illumination time for ir radiation. A reasonable fit to the points is obtained using the equation suggested by Lacklison *et al.*,[3] i.e.,

$$n_T = n_T^0 + \Delta n_T [1 - \exp(-kI)] , \quad (1)$$

where $n_T^0$ is the initial density, $\Delta n_T$ the maximum density change caused by the radiation, $I$ the integrated sample irradiation, and $k$ a constant. Lacklison *et al.* have observed similar behavior in their data and have suggested as a possible explanation that the excitation of *DX* centers proceeds as a random process and continues until all centers are ionized. However, as noted by Lacklison *et al.*, this interpretation is not entirely consistent since the total number of Si impurities in $Al_xGa_{1-x}As$ is much larger than $n_T^0 + \Delta n_T$ (by roughly a factor of 5). Falt *et al.*[2] have attributed a similar discrepancy in their data to a parallel conducting path in the $Al_xGa_{1-x}As$ layer. This model cannot be appropriate to the present samples because the resistivity $\rho_{xx}$, at high magnetic fields after illumination with ir radiation, shows an accurate zero up to $n_T \sim 10^{16}$ $m^{-2}$ in the case of sample 1 and up to about $9.5 \times 10^{15}$ $m^{-2}$ for sample 3. In addition, data on a sample from the same wafer of sample 3 (Harris *et al.*[1]) shows a zero when saturated with red light and so we conclude that the parallel conducting path is not present in our samples. Falt *et al.*[2] also observed an unusual behavior of the mobility as a function of $n_T$ which we do not find in the present work.

The increase in $n_T$ with red light does not obey Eq. (1), as shown in Fig. 1(b) for the three samples. Initially $n_T$ increases very rapidly, but this stage abruptly ends and is followed by a response which is 1–2 orders of magnitude weaker. We believe the initial steep increase in $n_T$ is caused by the generation of *e-h* pairs in the GaAs, whereby the holes neutralize the negatively charged acceptors in the GaAs depletion layer, and the electrons join the

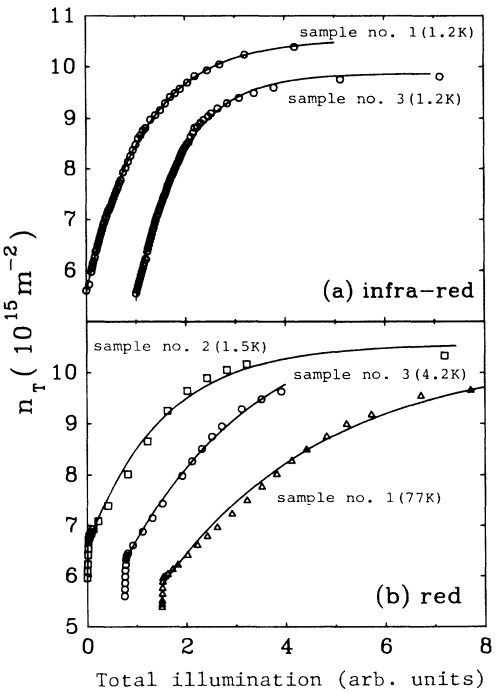


FIG. 1. (a) Total areal carrier densities $n_T$ as a function of integrated ir illumination (in arbitrary units) for samples 1 and 3. The data for sample 3 have been shifted by one unit along the abscissa. The solid lines are the best fits to Eq. (1) of the text and appear to give acceptable fits to the data. (b) Total areal densities $n_T$ as a function of integrated red illumination (in arbitrary units) for all three samples. The unit of radiation is unrelated to that in (a). The data for samples 3 and 1 have been shifted by 0.75 and 1.5 units along the abscissa. The solid lines are the best fits with Eq. (1), using only data after the initial abrupt rise; the quality of the fits is always much worse than for ir illumination. Although the data are taken at various temperatures, all our results suggest that temperature (in the range up to 77 K) has no effect on observed behaviors.

2D EG. This process ends when the GaAs depletion layer has disappeared (presumably the acceptors remain ionized in the region occupied by the 2D EG, extending a few hundred Å from the interface). If this explanation is correct, then the initial areal depletion charge $n_a$ in the GaAs is just equal to the initial abrupt change in the carrier concentrations in Fig. 1(b), and is about 0.55, 0.79, and $0.73\times10^{15}$ m$^{-2}$ for samples 1, 2, and 3, respectively (each $\pm\sim0.05\times10^{15}$ m$^{-2}$). This technique seems to offer a particularly simple and effective way of characterizing a particular heterojunction with respect to $n_a$; we have also observed the same effects in samples with single-band occupancy. Of course, if the sample is partially compensated, this measurement provides the difference between the acceptor and donor concentrations in the GaAs.

If the acceptors were confined to 1 $\mu$m of undoped GaAs, these results imply net impurity concentrations of $N_a\sim(5-8)\times10^{20}$ m$^{-3}$. An alternative estimate of $N_a$ is based on equilibrium considerations. The samples were all cooled slowly and so, in the dark, one would expect the chemical potential $E_F$ to be the same throughout the junction region. Since $E_F$ is pinned to the GaAs acceptor levels well away from the junction, and to the bottom of the conduction band (within 0.2 eV) at the junction, the total band bending amounts to the energy gap $E_g$ of GaAs, i.e., about 1.5 eV. Assuming a uniform depletion charge density $N_a$, then $E_g\sim N_a W_a^2 e^2/2\epsilon\epsilon_0$, where $W_a$ is the width of the acceptor depletion layer and $\epsilon$ the dielectric constant. Hence $n_a\sim(2E_g\epsilon\epsilon_0 N_a/e^2)^{1/2}$ and so $N\sim(1.5-3)\times10^{20}$ m$^{-3}$ if we use $n_a$ as obtained above. This estimate yields $W_a\sim3-4$ $\mu$m which is much larger than the width of the grown GaAs and suggests that the depletion layer must enter into the substrate. Which of these two pictures, if either, is correct is difficult to decide but the interpretation of the data as yielding a measure of $n_a$ is supported independently by the theoretical calculations to be described later.

After the acceptor depletion layer has been neutralized, the further production of *e-h* pairs by the red light is followed by recombination and we can explain the continued increase of the 2D EG density only in terms of *DX*-center ionization. In other words, further illumination should act in the same way as ir radiation and one might expect an exponential rise in $n_T$ according to Eq. (1). Figure 1(b) shows that this is *not* observed. Immediately following the initial abrupt rise, the increase in $n_T$ is better represented by a straight line rather than an exponential. [It should be noted that the exponential fits in Fig. 1(b) were made by neglecting the data below the knee to better conform to the explanation presented above.] The behavior seen in Fig. 1(b) does not seem to have been observed by Lacklison *et al.*[3] in a study carried out at 77 K with 2.2-eV photons. We have also checked sample 1 at 1.2 K but the data show no significant differences and so we present only 77 K data for this sample in Fig. 1(b). As a variation on the experiment, we initially illuminated sample 1 with red light but switched to ir immediately following the abrupt knee. We were surprised to find that the resulting $n_T$ as a function of illumination is very similar to that obtained with red light in Fig. 1(b), i.e.,

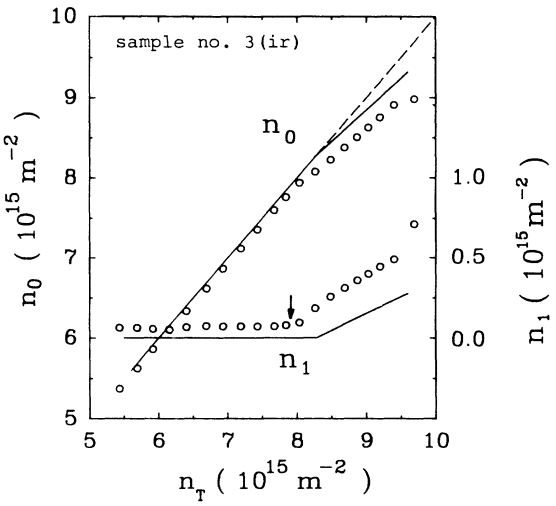


FIG. 2. The areal carrier densities $n_i$ for the two subbands as a function of total density $n_T$ for sample 3 with ir illumination. The lines through the points are from the calculations. The vertical arrow at $(7.95\pm0.5)\times10^{15}$ m$^{-2}$ corresponds to the first observation of $n_1$ for comparison with Fig. 4(b). Notice the scale change for $n_1$. The data were taken at 1.2 K.

even in this case Eq. (1) is not appropriate to the data. Apparently prior treatment of the sample with red light has modified the way in which electron generation by *DX*-center ionization, or electron accumulation in the 2D EG, proceeds.

Because we have measured the dHS oscillation frequencies of the first band in our experiments, we have detailed information about the densities of electrons in each subband, $n_0$ and $n_1$ (the latter being obtained from $n_T-n_0$ as discussed earlier). Figures 2 and 3 show these data for both ir and red illumination in the case of sample 3; data for sample 1 are similar. We do not have data for sample 2 with red illumination, but those for ir are very similar to that of Fig. 2. It is evident that the curves are quite different for the two kinds of illumination, a feature not apparent in earlier experimental results[1] which used a

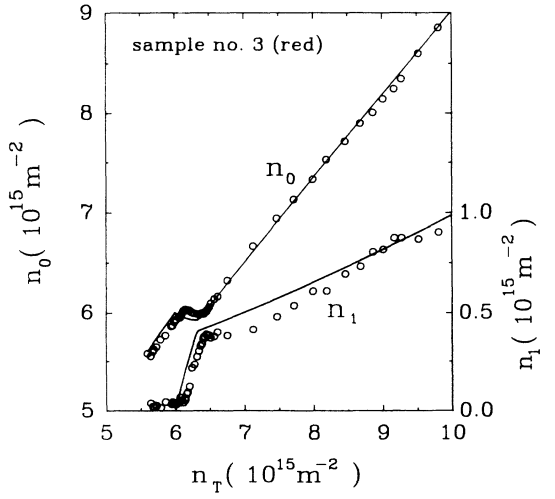


FIG. 3. As Fig. 2 but with red light.

different technique to evaluate $n_1$. With ir radiation, $n_1$ increases smoothly with $n_T$ through the whole range, and $n_0$ shows a modest change of slope where $n_1$ begins to increase. By contrast, with red illumination there is an abrupt onset of $n_1$ followed by another abrupt change of slope when $n_1$ reaches about $0.3\times10^{15}$ m$^{-2}$, after which $n_1$ changes only slowly with $n_T$. The differences in behavior arise from the ability of the red light to decrease the number of charged acceptors in the GaAs as mentioned earlier; for each photon absorbed a positive acceptor is converted to a neutral atom with an electron added to the 2D EG. This process ends when all the acceptors are neutralized and this corresponds to the change of slope of $n_1$ versus $n_T$. The details of this picture are worked out in Sec. IV and confirm these interpretations.

We now turn to the variation of the transport mobility $\langle\mu\rangle$ (the angular brackets implying an average over two bands where appropriate) with $n_T$. The relevant data are shown in Figs. 4(a) and 4(b) for samples 2 and 3 (sample 1 is omitted because it is similar to sample 2). As with $n_1$ and $n_0$ the detailed behavior of $\langle\mu\rangle$ is seen to be quite different for the red and ir illumination. In both cases, the initial linear rise of $\langle\mu\rangle$ with $n_T$ is followed by a rapid decrease due to the onset of intersubband scattering but the position at which this drop appears is at a much lower value of $n_T$ for red illumination as compared to ir (cf. Figs. 2 and 3 for the initial appearance of $n_1$). This difference in position is consistent with the model outlined above (see also Harris *et al.*[1]).

There are other differences that were not visible in earlier data.[1] For example, we see that the width of the region over which the mobility drops is much wider for ir than for red. In a previous publication[14] we identified the width of the transition region for the ir case as being a measure of the width of the tail in the density of states at the bottom of the second subband. For ir radiation this width (measured from the maximum to minimum of $\langle\mu\rangle$) is very similar for all samples at about $0.9\times10^{15}$ m$^{-2}$. On the other hand, the mobility drop for red light is much steeper than for ir and occurs over the range $(0.1-0.2)\times10^{15}$ m$^{-2}$. One might be tempted to conclude that the tail in the density of states is different for the two kinds of illumination, but this inference is not correct. The observed widths actually reflect the rate at which $E_F-E_1$ is changing with $n_T$ where $E_F$ is the 2D EG Fermi level and $E_1$ the energy of the bottom of the upper subband; as we will show in Sec. IV C, this rate is much higher for red light and so the tail appears to be much narrower. It should be noted that, with red light, the effect of the end of the acceptor depletion layer neutralization is also noticeable on $\langle\mu\rangle$. After the minimum in $\langle\mu\rangle$ one sees an initial rapid rise in $\langle\mu\rangle$ followed by a slower rate of increase [e.g., Fig. 4(a) for sample 2 near $n_T\sim(6.6-6.8)\times10^{15}$ m$^{-2}$]. This effect is also visible for sample 3 but not for sample 1. For sample 1 the end of the depletion layer coincidentally takes places as $\langle\mu\rangle$ is dropping (i.e., coincident with the appearance of $n_1$) and so the effect is hidden; this is consistent with the lower value of $n_a$ for this sample. We note that the experimental data are noticeably unstable in the region corresponding to the end of $n_a$ which may be due to electrons from the 2D EG falling back into GaAs acceptor levels, as a consequence of the extended wave function of the upper subband in the almost flat potential. Otherwise, except when close to saturation, the data are extremely stable, e.g., the resistivity is constant to $<0.1\%$ for time periods

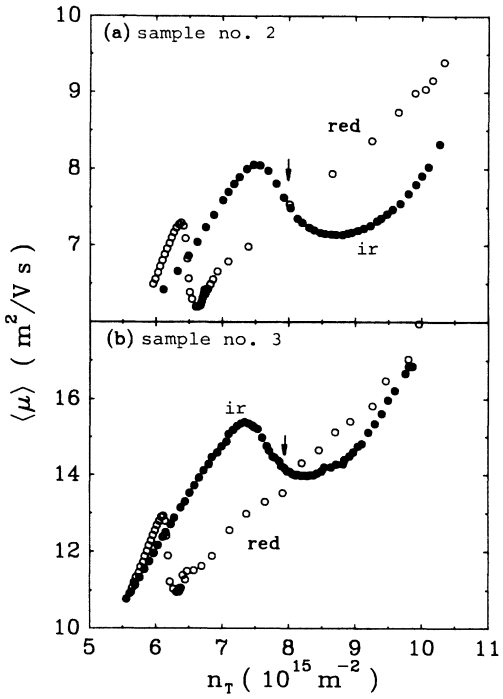


FIG. 4. (a) The measured mobility $\langle\mu\rangle$ as a function of total areal density $n_T$ for sample 2 for both red (open circles) and ir illumination (closed circles): the temperature is 1.2 K. The vertical arrow corresponds to the first observations of $n_1$. (b) As Fig. 4(a) but for sample 3. The arrow is in the same position as in Fig. 2.

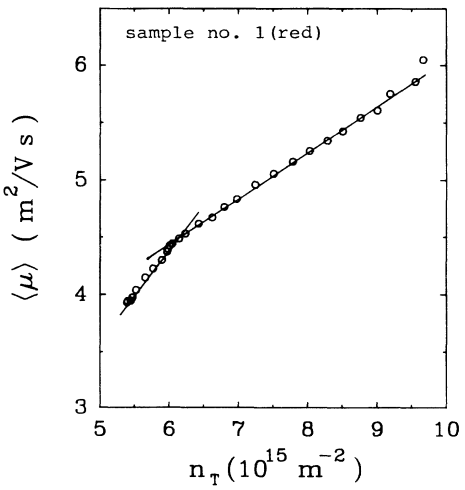


FIG. 5. The measured mobility $\langle\mu\rangle$ for sample 1 as a function of total areal density with red light measured at 77 K. The lines are meant as a guide to the eye; notice the change of slope near $n_T=6\times10^{15}$ m$^{-2}$ marking the end of the ionized acceptor depletion charge.

of the order of 12 h for $T \leq 4.2$ K.

Interestingly, it is much easier to detect the effect of eliminating the acceptor depletion layer on $\langle \mu \rangle$ versus $n_T$ at higher temperature. Thus Fig. 5 shows an example of such data for sample 1 at 77 K with red illumination. We no longer observe any decrease due to the second-band occupancy because the available thermal energy $kT$ allows this band to be populated much more smoothly as a function of $n_T$ than at 1.2 K. However, we still observe a discontinuity in the slope of $\langle \mu \rangle$ versus $n_T$. This corresponds to the abrupt knee in Fig. 1(b) for the same sample and signals the end of the GaAs depletion layer. Below this point the depletion layer is shrinking and the well is becoming broader as $n_T$ rises. The opposite is true above that point leading to the discontinuity in slope.

We would also like to emphasize a feature of the ir data for sample 3 in Figs. 2 and 4(b) which was noticed earlier with respect to sample 1.[14] The electron density $n_T$ at which carriers are first seen in the upper subband [indicated by the vertical arrow at $7.95 \times 10^{15}$ m$^{-2}$ on Figs. 2 and 4(b)] corresponds to a point well beyond the peak in $\langle \mu \rangle$ (which occurs at $7.25 \times 10^{15}$ m$^{-2}$). The gradual decrease in $\langle \mu \rangle$ due to intersubband scattering must be associated with an increasing density of states in the upper subband and yet over the range $(7.25-7.95) \times 10^{15}$ m$^{-2}$ no carriers in the second subband are revealed by Hall resistivity measurements. The same feature is also present in the red illumination data in Figs. 3 and 4(a) but is less obvious since the drop in $\langle \mu \rangle$ occurs over a narrower range of $n_T$. However all data on all samples are consistent with the result that $n_1$ does not appear until $\langle \mu \rangle$ is approaching its minimum value.

We suggested previously[14] that this is due to the lowest energy states in the upper subband being localized and therefore not contributing to $n_T$. There is another independent feature in our data which points to the same explanation. If we expand the graphs of the initial abrupt increase of $n_T$ as a function of red illumination [Fig. 1(b)] we observe the results shown in Fig. 6. The data both above and below the knee exhibit a good linear dependence of $n_T$ as a function of total illumination except that there is usually a distinct nonlinear region just below the knee. The nonlinearity always appears just after the peak in the $\langle \mu \rangle$ versus $n_T$ curve and reaches a maximum deviation near the point of inflection of $\langle \mu \rangle$: the arrows on Fig. 6 give the peak and valley positions of $\langle \mu \rangle$ for each sample. The effect is not visible for sample 1 because this region straddles the knee of the illumination curve. The nonlinearity is in such a direction that the observed $n_T$ is smaller than a linear extrapolation of lower illumination data would lead us to expect. Again, the simplest explanation for this feature is that some of the electrons are in localized states at the bottom of the upper subband, and these make no contribution to $\rho_{yx}$ and hence $n_T$. Of course, the same features could equally well result from a very low mobility of the electrons in the tail of the upper subband. One can make this more quantitative by noting that the Wilson two-band model[15] referred to earlier predicts that the deviation of $n_T$ from the linear extrapolation varies from 0 to $n_1$ as $\omega_c \tau_1^t$ decreases from $\sim 1$ to $\ll 1$ (provided the high-field limit is satisfied for the electrons in the lower subband, i.e., $\omega_c \tau_0^t \gg 1$). Detailed numerical estimates suggest that $\mu_1$ must be less than about 1 m$^2$/V s to produce the observed behavior. Since there is a definite tendency for the points in Fig. 6 to recover towards the linear extrapolation at higher total illumination the upper subband electrons must become more mobile and enter the high-field limit as their numbers increase.

## IV. THEORY AND DISCUSSION

The interpretations that we have given for the various experimental results (except for band tailing effects) are supported by detailed calculations of both the electronic structures and mobilities of the heterojunctions. As input to the mobility calculations we require the distribution of ionized charge in the $Al_xGa_{1-x}As$; at the present time we have incomplete knowledge of this distribution which leads to uncertainties in the final results. Nevertheless, some useful information concerning restrictions on the arrangement and amount of ionized charge does emerge from the calculations. Fortunately, these details do not significantly affect the results of the electronic structure calculations which are thus quite unambiguous; we deal with this aspect first.

### A. Self-consistent electronic structure

The electronic structure of the heterojunction was determined using the density-functional method as de-

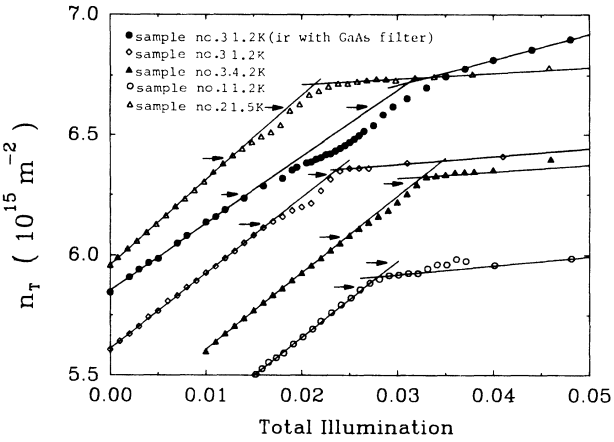


FIG. 6. The total areal density $n_T$ (measured by $\rho_{yx}$) as a function of integrated red illumination showing only data taken near the end of the acceptor depletion layer (which is indicated by the change of slope); lines have been drawn through the data using least mean-squares linear fits to data below the knee (omitting the nonlinear region) and above the knee [cf. Fig. 1(b)]. The horizontal scale has the same units as Fig. 1(b) and for clarity the data for samples 1 and 3 (at 4.2 K) have been shifted to the right by 0.01 units. All data are appropriate to the red diode, except for sample 3 (closed circles) which were taken with the ir diode and GaAs filter, a combination which leaks a small of amount of red light. The pair of arrows on each set of data correspond to the observed maximum and minimum values of $\langle \mu \rangle$.

scribed by Stern and Das Sarma[13] (SDS). The conduction-band offset at the $Al_xGa_{1-x}As/GaAs$ interface was taken to be 0.28 eV (Ref. 16) ($0.68\,\Delta E_g$) but the results are not very sensitive to small changes in this value since there is relatively little wave-function penetration into the barrier region. A spacer of width $s$ separates the region of ionized Si donors from the interface. To obtain the electric field confining the electrons to the interface, it is sufficient to assume the ionized donors to have a total areal density $n_d$. Similarly the acceptors in the GaAs are taken to have a uniform volume density $N_a$ and to form a negatively charged depletion layer extending out a distance $W_a$ from the interface with a total areal density $n_a = N_a W_a$. Red illumination data provides $n_a$, and $N_a$ is estimated from the expression $N_a = (n_a e)^2/2E_g\epsilon\epsilon_0$ (Sec. III), e.g., $N_a = 2.40\times10^{20}$ m$^{-3}$ for sample 3. The measured value of $n_T$ for the equilibrium condition of the junction then allows one to determine the corresponding density of the ionized donors from the charge neutrality condition $n_d = n_T + n_a$.

The subband wave functions are obtained from a self-consistent solution of the one-dimensional Schrödinger equation

$$-\frac{\hbar^2}{2m^*}\frac{d^2\psi_i(z)}{dz^2} + V_{\text{eff}}(z)\psi_i(z) = E_i\psi_i(z)\ , \tag{2}$$

where the electronic band mass in $m^* = 0.067m_e$ and where the effective potential is given as a sum of electrostatic and exchange-correlation contributions:

$$V_{\text{eff}}(z) = V_H(z) + V_{\text{xc}}(z)\ . \tag{3}$$

$V_H(z)$ is obtained from the solution of Poisson's equation

$$\frac{d^2V_H}{dz^2} = \frac{e^2}{\epsilon\epsilon_0}[n^{\text{ext}}(z) - n(z)]\ , \tag{4}$$

where $n^{\text{ext}}(z)$ represents the (positive) external charge density in the junction and $n(z) = \sum_i n_i|\psi_i(z)|^2$. The electrostatic potential is screened by the GaAs dielectric constant $\epsilon = 13.2$. For the exchange-correlation potential, we use the local density approximation as given by SDS. The above parameter values yield an effective Bohr radius $a^* = 4\pi\epsilon\epsilon_0\hbar^2/m^*e^2 = 10.42$ nm and an effective Rydberg $\text{Ry}^* = m^*e^4/32\pi^2\epsilon^2\epsilon_0^2\hbar^2 = 5.23$ meV.

Neither the dielectric constant nor the band mass was allowed to vary through the interface. As shown by SDS, such refinements are only of secondary importance. The accuracy of our calculations was confirmed by a comparison with their results. For example, we find a subband separation of $E_{10} = 26.11$ meV and an average distance of the electrons in the lowest subband from the interface of $\langle z\rangle_0 = 6.695$ nm, using $N_a = 3\times10^{20}$ m$^{-3}$, $n_a = 0.8\times10^{15}$ m$^{-2}$, $n_T = 5\times10^{15}$ m$^{-2}$, $m^* = 0.07m_e$, and $\epsilon = 13.0$. This is to be compared with the SDS values of 26.18 meV and 6.696 nm, respectively, for the same set of junction parameters.

The effect of illumination on the subband states is simulated in the following way. ir radiation is assumed to create positively charged centers in the $Al_xGa_{1-x}As$ and are accounted for in the self-consistent calculations by expanding the ionized donor region in proportion to the density of photogenerated carriers. The equilibrium (i.e., initial) value of $n_T$ in sample 3 is $5.6\times10^{15}$ m$^{-2}$ and this is progressively increased to $10\times10^{15}$ m$^{-2}$. The corresponding areal donor density $n_d$ increases from $6.33\times10^{15}$ m$^{-2}$ to $10.73\times10^{15}$ m$^{-2}$. In Fig. 7(a) we show the subband energies $E_0$ and $E_1$ relative to the Fermi level as a function of $n_T$. The subband separation $E_{10}$ increases with $n_T$ as a result of the narrowing of the confining potential well and reflects the increasing interface electric field due to the increasing donor charge density. The second observation of interest is the point at which the second subband energy crosses the Fermi level $E_F$. In our calculations this occurs at a density of $7.4\times10^{15}$ m$^{-2}$ for sample 1 and $8.3\times10^{15}$ m$^{-2}$ for sample 3 which are somewhat higher than the respective values of about $7.2\times10^{15}$ and $8.0\times10^{15}$ m$^{-2}$, indicated by the mobility data. However, considering the uncertainties in some of the experimental parameters, particularly $n_a$, as well as the theoretical approximations (e.g., the local density approximation), the agreement is really quite good and confirms that calculations of this kind do provide a realistic description of the electronic properties. In Fig. 2 we also show the subband densities $n_0$ and

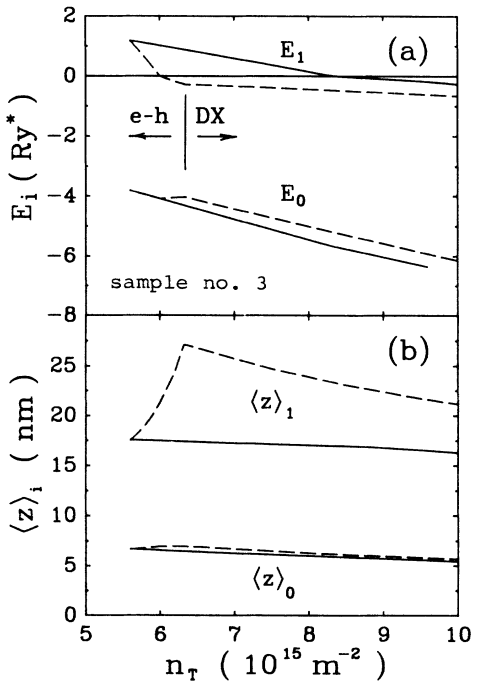


FIG. 7. (a) The calculated subband energy minima $E_0$ and $E_1$ as a function of the total areal density $n_T$ for sample 3. The ordinate is given in effective rydbergs (1 $\text{Ry}^* = 5.23$ meV) relative to the Fermi level $E_F$. The solid and dashed lines are for ir and red illumination, respectively. In the latter case the vertical line at $6.33\times10^{15}$ m$^{-2}$ indicates the point at which the acceptor depletion layer becomes exhausted, after which only $DX$-center excitation is assumed to contribute to $n_T$. (b) The mean distances $\langle z\rangle_i$ from the interface of the electrons in the two bands for the same cases as Fig. 12(a).

$n_1$ versus $n_T$. As discussed in our earlier paper,[14] $n_1$ is suppressed as a result of the increasing subband separation $E_{10}$ and explains why $n_0$ displays only a slight kink at the onset of second subband occupancy. If the confining potential was independent of density, the rate of increase of $n_0$ with $n_T$ would of course be one-half its value below the onset point.

The situation of red illumination is modeled by initially decreasing the width of the negative depletion layer in the GaAs to compensate for the excess electron density. Decreasing the interface electric field with increasing $n_T$ leads to a decreasing subband separation as shown in Fig. 7(a) and as a result, the second subband first becomes occupied at a lower total density, $5.75\times10^{15}$ m$^{-2}$ in the case of sample 1 and $6.0\times10^{15}$ m$^{-2}$ in the case of sample 3. This is again in reasonable quantitative agreement with the experimental data although now the theoretical onset values are slightly below the experimental values. A partial explanation might be that red illumination is also ionizing *DX* centers in the $Al_xGa_{1-x}As$ as in the case of infrared radiation. The illumination data [Figs. 1(a) and 6] show that this happens but with a much lower efficiency than *e-h*-pair generation. Allowing for this possibility in the calculations would shift second subband occupancy to higher densities.

The maximum increase in $n_T$ achievable with *e-h*-pair excitation is approximately the total depletion charge density $n_a$. For sample 3 this gives a limiting density of $6.33\times10^{15}$ m$^{-2}$, slightly above the point at which the second subband is occupied. By eliminating the depletion layer the self-consistent potential saturates at a constant value beyond the region of the electron gas with $E_F$ just below this level. The fact that the electron density cannot be increased further by this mechanism is presumably due to the recombination of the generated *e-h* pairs and corresponds to the saturation point observed in the illumination data with red light. Since the confining potential barrier on the GaAs side of the junction is reduced considerably by this process, the second subband wave function is much more extended than for the equilibrium configuration. As shown in Fig. 7(b), its mean extent $\langle z\rangle_1$ from the interface increases from 17.6 to 27.1 nm through the *e-h*-pair generation phase. The effect on the first subband state is much less pronounced as it is confined by the inner part of the potential and is less sensitive to the electrostatic barrier provided by the depletion layer. In Fig. 3 we show the subband densities versus $n_T$. In this case, the first subband actually depopulates slightly when the second subband is being filled. This result is in accord with the experimental findings.

Following completion of the *e-h*-pair generation phase, $n_T$ continues to increase as a result of *DX*-center ionization. The continuation of the curves in Figs. 7 and 3 beyond $6.33\times10^{15}$ m$^{-2}$ is based on this picture and is again in accord with the observed behavior.

In summary, the electronic structure calculations performed support the interpretation given to the illumination data. In particular, the good agreement in the second subband onsets and variation of subband densities with $n_T$ provide substantial evidence for the proposed excitation mechanisms.

### B. Junction electrostatic

As we have mentioned in the introduction to Sec. IV, the calculation of mobility requires knowledge of the spatial distribution of ionized donors within the $Al_xGa_{1-x}As$. This in itself is a complex and difficult problem and in an earlier paper we made the simplifying assumption that the donor depletion layer contained a density $N_d$ of ionized donors equal to the Si doping density and extending a distance $W_d$ into $Al_xGa_{1-x}As$ from the edge of the spacer. This model may be appropriate to a semi-infinite $Al_xGa_{1-x}As$ layer but is inadequate for the real situation of a thin layer capped with another layer of GaAs. In this latter situation one needs a more realistic estimate of the spatial distribution of ionized donors for both the equilibrium conditions and also under illumination.

To determine the equilibrium distribution of ionized impurities we adopt a model[17] which invokes two species of donors, the usual shallow hydrogeniclike states, and also the deep *DX* center.[5–9] The relative proportions of the two types of donor, and their energies relative to the conduction-band edge are important parameters determining the equilibrium junction properties, and both are still subjects of ongoing research. We shall make the assumption that on initial cooldown the junction is in thermodynamic equilibrium. There is some evidence[18] that the *DX* centers cannot reach equilibrium below about 120 K but how this is to be included is unclear at the present time. Along with the geometry related parameters listed in Table I, we assume a conduction-band offset of 0.28 eV,[16] a shallow donor density of $N_{sd}$ (with energy just below the conduction-band edge), and a deep donor density $N_{dd}$ with energy $E_{dd}$, again referred to the conduction-band edge. The total donor density $N_d=N_{sd}+N_{dd}$ is taken to be equal to the Si doping density. In addition we assume $E_F$ to be pinned midgap at the surface of the GaAs cap layer, and to be constant throughout the system (i.e., a condition of thermodynamic equilibrium). The self-consistent calculation of the

TABLE I. Sample parameters as determined during molecular-beam-epitaxial growth.

| | GaAs cap Layer (Å) | $Al_xGa_{1-x}As$ $x$ | Width (Å) | Si dopant ($10^{24}$ m$^{-3}$) | Undoped spacer (Å) | GaAs ($\mu$) |
|---|---|---|---|---|---|---|
| samples 1 and 2 (G130) | 200 | 0.34 | 400 | 1.32 | 0 | 1 |
| sample 3 (G131) | 200 | 0.33 | 400 | 1.34 | 16.7 | 1 |

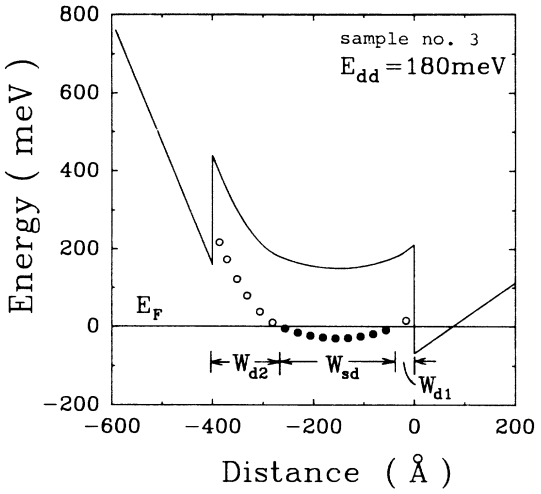


FIG. 8. The calculated position of the conduction-band edge (relative to $E_F$) through the junction region for sample 3 with $E_{dd}=180$ meV under equilibrium conditions. The curve between 0–200 Å is a simple triangular approximation and does not take the presence of the electrons into account. The circles represent deep donor levels which are either neutral (solid circles) or ionized (open circles); the shallow donors are completely ionized and are not shown. Table II and the text give more information about this and other cases.

electronic states within the quantum well [as dealt with in Sec. 4(a)] provides the position of $E_F$ relative to the conduction band at the $Al_xGa_{1-x}As/GaAs$ interface; this value, together with the known charge in the GaAs (i.e., both electronic and ionized acceptors) determines the electrostatic boundary condition at this interface. The displacement field is taken to be continuous at all interfaces, and a dielectric constant of 12.2 was used for $Al_{0.33}Ga_{0.67}As$. Finally, we take the shallow donors to lie above $E_F$ and therefore to be completely ionized; if this were not so we would anticipate a problem with parallel conduction in $Al_xGa_{1-x}As$ which is not observed for these junctions.

With the above assumptions one can solve Poisson's equation and determine the position of the conduction-band edge throughout the system for various values of the parameters $E_{dd}$ and $N_{sd}/N_{dd}$. In our model there is no solution for any value of $N_{sd}/N_{dd}$ when $E_{dd}<170$ meV (for sample 3) because for this situation the interface boundary condition dictates that the deep donors are completely ionized and it is impossible to satisfy the boundary condition at the surface of the cap layer. (As we shall see later, a situation in which all donors in the $Al_xGa_{1-x}As$ are completely ionized is also incompatible with the observed mobility.) When $E_{dd}>170$ meV, the deep level begins to fall below $E_F$ and a self-consistent solution becomes possible for a particular value of $N_{sd}/N_{dd}$. This ratio increases steadily from a value of 0.13 at $E_{dd}=175$ meV to about 0.5 at $E_{dd}=210$ meV. For $E_{dd}=180$ meV, $N_{sd}/N_{dd}\sim 0.27$; the variation of the conduction-band edge through the system is shown in Fig. 8 for this case. Table II lists the widths and areal densities of the various donor depletion layers for both this case, and some other cases of interest.

The minimum value of $E_{dd}$ that we require, i.e., 170 meV, is much larger than the frequently quoted result of about 100 meV which is based on the analysis[5] of the temperature dependence of the Hall resistivity in bulk $Al_xGa_{1-x}As$. In our model $E_{dd}$ can be reduced only by lowering the conduction-band offset. However, the value of the offset is well defined experimentally[16] and so this option seems to be untenable. It is possible that the literature value of $E_{dd}$ is in error by a factor of 2 due to ambiguities in the analysis.[9] A recent analysis of similar experimental data[7,8] has raised the value of $E_{dd}$ to 140 meV, but this still falls short of our minimum requirements. It is also possible that there is actually a distribution of energy levels, and the thermal analysis is weighted towards the shallower states. Nevertheless, the discrepancy is unsettling and suggests that the model of two discrete donor states is incomplete or unsatisfactory in some way. The other parameter $N_{sd}/N_{dd}$ has a much wider range of possible values, being sensitive to both the

TABLE II. Areal densities $n$ (in units of $10^{15}$ m$^{-2}$) and widths $W$ (Å) of the various donor depletion layers together with the resultant mobilities $\langle\mu\rangle$ for different values of the depth of the deep donor level $E_{dd}$ and ratio of shallow-deep donor concentration $N_{sd}/N_{dd}$ required for thermal equilibrium. The results are appropriate to sample 3 in thermal equilibrium with a conduction-band offset $\Delta E_c=280$ meV, 2D EG density $n_T=5.6\times10^{15}$ m$^{-2}$, and spacer layer width $s=16.7$ Å. The subscripts have the following significance (c.f. Fig. 8): $d1$ the first completely ionized layer adjacent to the spacer; $sd$ the next layer with only shallow donors ionized; $d2$ the last layer reaching up to the cap/$Al_xGa_{1-x}As$ interface in which all donors are again ionized.

| $E_{dd}$ (meV) | $W_{d1}$ | $n_{d1}$ | $W_{sd}$ | $n_{sd}$ | $W_{d2}$ | $n_{d2}$ | $N_{sd}/N_{dd}$ | $\langle\mu\rangle$ (m$^2$/V s) |
|---|---|---|---|---|---|---|---|---|
| 170 | | | | no equilibrium solution | | | | |
| 175 | 35.3 | 4.73 | 213 | 3.2 | 152 | 20.3 | 0.127 | 4.99 |
| 180 | 21.8 | 2.92 | 240 | 6.8 | 138 | 18.5 | 0.269 | 5.61 |
| 185 | 13.3 | 1.79 | 257 | 9.1 | 130 | 17.4 | 0.359 | 6.29 |
| 190 | 6.6 | 0.88 | 271 | 10.9 | 123 | 16.5 | 0.430 | 7.17 |
| 195 | 0.8 | 0.11 | 282 | 12.5 | 117 | 15.7 | 0.491 | 8.45 |
| 200 | 0 | 0 | 286 | 12.9 | 115 | 15.3 | 0.506 | 8.62 |
| 205 | 0 | 0 | 288 | 13.1 | 112 | 15.0 | 0.514 | 8.55 |

Al content and the sample preparation.[6,8] At $E_{dd}=180$ meV, the total ionized areal density is $2.8\times10^{16}$ m$^{-2}$ which is larger than $n_T+n_a=6.3\times10^{15}$ m$^{-2}$ (for sample 3, but the others are similar). Within this model, the difference of $2.2\times10^{16}$ m$^{16}$ m$^{-2}$ resides in surface states at the surface of the GaAs cap. The density of neutral donors, $2.5\times10^{16}$ m$^{-2}$, which is presumably the source of PPC, is much higher than the observed increase of 2D EG density with illumination ($\sim0.5\times10^{16}$ m$^{-2}$). The precise numbers will change for different assumed values of $E_{dd}$; nevertheless, there is an abundance of potentially available charge to satisfy the observed PPC. The details of what might happen under illumination are best left until we consider the mobility, because this is no longer an equilibrium situation and so goes beyond the scope of this section.

### C. Mobility

The mobility was calculated using the self-consistent subband wave functions to evaluate transition-matrix elements. In view of the good agreement with observations that has been found in Sec. IV A we believe these to be very reliable and any errors in the final results must be due to other sources. Details of the transport calculations are given in the Appendix. Here we restrict ourselves to a summary of the assumptions and some of the numerical results. In addition to the ionized donors, we also take into account scattering by the ionized acceptors in the GaAs but these have a negligible effect on the results. To obtain transport lifetimes we have used the formulation of multiband transport due to Siggia and Kwok.[19] The scattering rates entering the Boltzmann equation were calculated in the Born approximation using screened impurity potentials which are configuration averaged.

Screening of the impurity potential is taken into account within a two-band model at the level of the random-phase approximation (linear response theory). This requires the calculation of the independent particle density response function of the 2D EG which includes both intrasubband and intersubband polarization processes. The intrasubband response function is the familiar Stern result;[20] an expression for the intersubband contribution is given in Eq. (A15) and has been used previously in other contexts.[21] In evaluating the dielectric matrix of the 2D EG [Eq. (A11)] the self-consistently determined numerical subband wave functions were used to evaluate the Coulomb form factors $F_{\alpha\beta}(q)$ of Eq. (A12). Previously, we used variational wave functions for this purpose,[14] but for the range of experimental conditions considered in this work, the more elaborate calculations were found to be necessary.

Table II shows the calculated $\langle\mu\rangle$ of sample 3, for various equilibrium conditions determined by $E_{dd}$, and indicates the sensitivity to the spatial distribution of ionized donors. $\langle\mu\rangle$ increases from 5.0 m$^2$/V s at $E_{dd}=175$ meV, reaches a maximum of 8.6 m$^2$/V s at $E_{dd}=200$ meV, and then decreases slowly at larger $E_{dd}$. This mainly reflects the number of ionized donors in the region closest to the interface ($W_{d1}, n_{d1}$) in that as the donor level is deepened the magnitude of the charge in this region decreases. For $E_{dd}=180$ meV, the ratio $N_{sd}/N_{dd}$ is 0.27 which is similar to the results obtained by Schubert and Ploog[7,8] for $x=0.33$. The resultant $\langle\mu\rangle$ (5.6 m$^2$/V s) is lower than that observed (10.7 m$^2$/V s) but it is difficult to say whether this discrepancy can be completely accounted for by errors in the assumed charged distributions, or whether some of it is inherent to the calculation; we will return to this point later.

It may be of interest to indicate the relative importance of the various donor regions in determining $\langle\mu\rangle$. At $E_{dd}=180$ meV the three donor charge layers have densities $n_{d1}=2.9\times10^{15}$ m$^{-2}$ (complete ionization next to the spacer), $n_{sd}=6.8\times10^{15}$ m$^{-2}$ (only shallow donors ionized), and $n_{d2}=18.5\times10^{15}$ m$^{-2}$ (complete ionization again). If $\langle\mu\rangle$ is calculated including each additional layer successively, starting from the interface, one obtains 7.9 , 6.0, and 5.7 m$^2$/V s. The slight decrease to the final value of 5.61 m$^2$/V s in Table II shows the minor effect of including the surface charge at the surface of the cap layer. It is also clear that it is the fully ionized layer adjacent to the spacer that primarily limits $\langle\mu\rangle$. If this layer is eliminated, e.g., by increasing $E_{dd}$ to 195 meV, $\langle\mu\rangle$ is then mainly determined by the ionized shallow donors and becomes much closer to the observed value.

As a final point of comparison we have calculated $\langle\mu\rangle$ assuming a uniform ionized donor layer with areal density $n_d=n_T+n_a=6.3\times10^{15}$ m$^{-2}$ and width 47.2 Å located adjacent to the spacer (of width 16.7 Å). These are the assumptions made in our earlier paper[14] and yield 5.0 m$^2$/V s. This is similar to the result obtained in the present more realistic case with distributed charge (having a total density of $28.3\times10^{15}$ m$^{-2}$).

We now turn to $\langle\mu\rangle$ versus $n_T$ as observed under illumination. In the case of ir radiation, we recall that we have associated the PPC effect with the ionization of deep donors, i.e., *DX* centers, in the $Al_xGa_{1-x}As$. Under equilibrium conditions, our model leaves about $2.2\times10^{16}$ m$^{-2}$ available for this process, which far exceeds the observed density increase in the quantum well of about $0.5\times10^{16}$ m$^{-2}$. There are a number of possible reasons why these numbers are so different.

(i) All remaining deep donors are ionized but the majority of electrons go to the surface of the GaAs cap layer.

(ii) The model overestimates the number of neutral deep donors remaining, or not all remaining donors can be ionized.

(iii) All deep donors are ionized but most of the photogenerated carriers remain in the vicinity of the ionized impurities. Since we do not observe any parallel conduction in these samples these carriers cannot be in the conduction band but must be trapped near the donors. In this event possibility (iii) is equivalent to (ii) in its consequences. It should be pointed out that a barrier prevents such recapture in bulk samples at low temperatures; we have no direct information about what happens in heterostructures.

Possibility (i) is the simplest to check. In the calculation we allow the remaining *DX* centers to be uniformly ionized with a fixed proportion ($\sim20\%$) going to the

quantum well so that by the end of the illumination process all donors are ionized. Curves 1a and 2a in Fig. 9 correspond to this scenario with two values of $E_{dd}$ for sample 3. They are clearly in poor agreement with the observations in Fig. 4(b); in particular $\langle \mu \rangle$ at the end of the process is a factor 4 lower than observed and this is just the case where the calculation should be the most reliable since there is no ambiguity in the charge distribution. These results appear to rule out the possibility that the final number of ionized impurities is equal to the Si donor density in the $Al_xGa_{1-x}As$.

The other possibility (ii) [and (iii) which is equivalent for our purposes] is modeled in two ways. In the first, the remaining deep donors are uniformly ionized to the extent required to provide the increase in electrons in the quantum well and the process ends when about 20% have been ionized. This results in curves 1b and 2b, Fig. 9, again for two values of $E_{dd}$. Finally we produce curves 1c and 2c under the assumption that the donor distribution remains fixed as a function of illumination. This is equivalent to our previous calculation[14] and might appear to be unrealistic but it could correspond to a redistribution of ionized donors. All these four curves represent the trend of the data much better and suggest that the number of ionized impurities is hardly changing with illumination. In Fig. 10(b) we present our results for sample 3 under red illumination. As we have already discussed (Sec. IV A), we assume that in the initial $e$-$h$-pair generation phase the acceptor depletion layer is eroded, and this is followed by $DX$-center ionization up to saturation. We show the results only for possibility (ii) discussed above with $E_{dd}=180$ meV and allow ionization of the deep donors to the extent required to provide the electrons in the 2D EG. We have also included the equivalent curve from Fig. 9 appropriate to ir illumination for comparison purposes.

Finally in Fig. 10(a) we present the calculations for sample 3 but only for the case comparable to sample 3 in Fig. 10(b) as discussed in the previous paragraph. In this case we used $E_{dd}=205$ meV and $N_{sd}/N_{dd}=0.2$ since there is no consistent solution satisfying the electrostatic boundary conditions for values of $E_{dd}$ less than about 205 meV. This is due to the slightly larger band offset (0.29 ev) and zero spacer width.

In all the above cases the discontinuity in the calculated $\langle \mu \rangle$ indicates the onset of intersubband scattering and is a consequence of the discontinuity in the assumed ideal 2D EG density of states. In reality the density of states is broadened by the random impurity potential and tails below the nominal subband edge. If this broadening is taken into account one would expect the continuous curve exhibited by the experimental data. We have not attempted to include disorder broadening in the calculations since a proper treatment goes beyond a simple Boltzmann transport theory description. Nevertheless we can comment on the narrowness of the mobility jump for red illumination as compared to the ir case. In density units, the widths as measured from maximum to minimum are $(0.1-0.2)\times10^{11}$ cm$^{-2}$ and $0.9\times10^{11}$ cm$^{-2}$, respectively, giving a ratio of about 6. This disparity is not inconsistent with our suggestion that the widths of

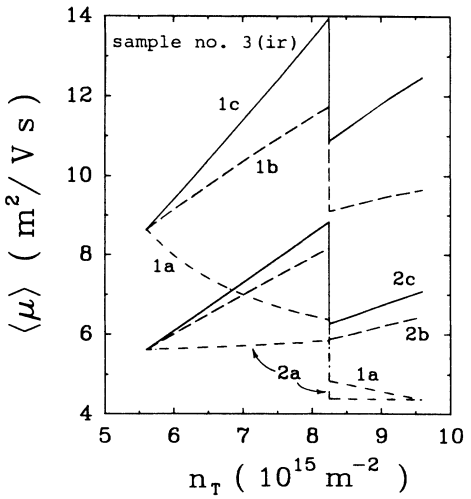


FIG. 9. The calculated mobilities $\langle \mu \rangle$ for sample 3 with ir illumination for the various scenarios discussed in the text. Briefly these are as follows. The upper set of curves 1a–1c correspond to $E_{dd}=200$ meV and the lower set (2a–2c) to $E_{dd}=180$ meV. The solid lines are for the case where the ionized donor concentrations are fixed, the dot-dashed lines to the case where all donors are ionized at saturation, and the dashed lines to an intermediate case.

the jump reflect the disorder broadening of the second subband density of states. Figure 7(a) shows that the second subband edge approaches the Fermi level at a rate which is 6.5 times faster for red as compared to infrared illumination and has the effect of reducing the width of

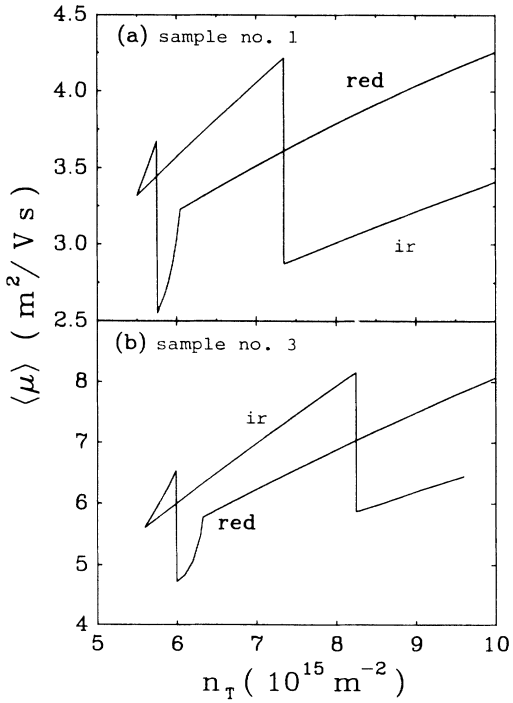


FIG. 10. (a) The calculated mobilities $\langle \mu \rangle$ for sample 1 for both red and ir illumination for the model discussed in the text with $E_{dd}=205$ meV. (b) As (a) but for sample 3 with $E_{dd}=180$ meV. The ir data are the same as those plotted in Fig. 9 (i.e., the dashed line with $E_{dd}=180$ meV).

the jump by the same factor. This is only a rough estimate, however, and a better comparison would see the inclusion of disorder broadening in the mobility calculations.

The behavior of $\langle \mu \rangle$ just above the point at which the second subband becomes occupied is interesting in that it is quite different for the two kinds of illumination. For red light the calculations show a narrow minimum in $\langle \mu \rangle$ versus $n_T$ [e.g., Fig. 10(b) near $6.0 \times 10^{15}$ m$^{-2}$]. This is reproduced in the experimental data for samples 2 and 3 [Figs. 4(a) and 4(b)], though it is not as pronounced as in the calculations which ignore disorder broadening. The origin of this feature is primarily the rapidly increasing contribution to $\langle \mu \rangle$ of the second subband electrons. As the acceptor depletion region is being eliminated, the second-band electrons become more extended and their contribution to $\langle \mu \rangle$ rises from zero as they just appear to about 15% of the total by the time the acceptor layer is exhausted. At this point there is an abrupt change of slope of $\langle \mu \rangle$ versus $n_T$ as *DX* excitation takes over. We also note that the initial slope of $\langle \mu \rangle$ versus $n_T$ is steeper for red light than for ir illumination in both the observations and calculations.

To summarize the situation: we see that all the trends exhibited by the observed $\langle \mu \rangle$ are well reproduced by the calculations appropriate to possibility (ii), i.e., that the ionized donor charge changes little with illumination. However, the calculations yield values that are uniformly too low, typically by a factor of 2. We can improve matters by adjusting various parameters such as $E_{dd}$ or the spacer width. The latter was done in our earlier work[14] but there is no sound reason for doing so. It is therefore difficult to decide whether the discrepancies we find are to be associated with errors in the assumed ionized impurity distribution or whether the mobility calculations themselves possess intrinsic limitations. We mention here various aspects which deserve further study. First, screening was determined within a two-subband model; it may be necessary to include all excited states of the quantum well to adequately represent the density response function. Second, exchange correlation was neglected in the screening process; its inclusion will enhance screening, but this is unlikely to be a significant effect. Finally, it is not at all obvious that a linear response treatment of the screening is adequate; it may well be that nonlinear corrections are significant, particularly for low mobility samples in which there are large fluctuations of the impurity potential.

### D. Transport and quantum lifetimes

Although this paper is not primarily concerned with electron lifetimes, there have been many experimental papers on two-band systems which contain data relevant to this situation.[15,22–27] The present section is significant in that it shows that red and ir illumination have very different effects on electron lifetimes, particularly for electrons in the second subband. We restrict the discussion to sample 3. In view of the fact that our model calculations produce mobilities which are too low, the lifetimes that we calculate will also be too low by roughly the same factor. However, we expect the general behavior as a function of type and quantity of illumination to be realistic. In a previous paper[14] we used similar calculations (with a fixed ionized donor distribution but with the spacer increased to give agreement with the observed mobilities) to give a good account of the behavior of the Dingle temperature, which reflects the quantum lifetimes, for sample 1 as a function of $n_T$.

Figures 11(b) and 12(b) show the transport lifetimes $\tau^t$ for both bands as a function of $n_T$ and evaluated for the model in which the number of ionized donors increases with the 2D EG density [i.e., possibility (ii) in Sec. IV C]. The lower subband lifetimes $\tau_0^t$ are similar for both red and ir, but the upper subband lifetimes $\tau_1^t$ generally differ by about an order of magnitude. The initial rapid rise in $\tau_1^t$ in the case of red light is due to the rapid extension of the wave function as the ionized acceptors are removed, and correlates with the behavior of $\langle z \rangle_1$ in Fig. 7(b). This rapid increase is also responsible for the narrow minimum in $\langle \mu \rangle$ versus $n_T$ [e.g., Figs. 10(a) and 10(b)] that was discussed in Sec. IV C. When the acceptor depletion layer has just disappeared the conductivity of the upper subband is about 15% of the total and this increases to about 20% at saturation. In contrast, with ir illumination, the upper subband contribution to the total conductivity is always negligible and the measured $\langle \mu \rangle$ is a direct measure of the transport lifetime of the first subband.

At the discontinuity corresponding to the occupation of the second subband the transport lifetime of the first

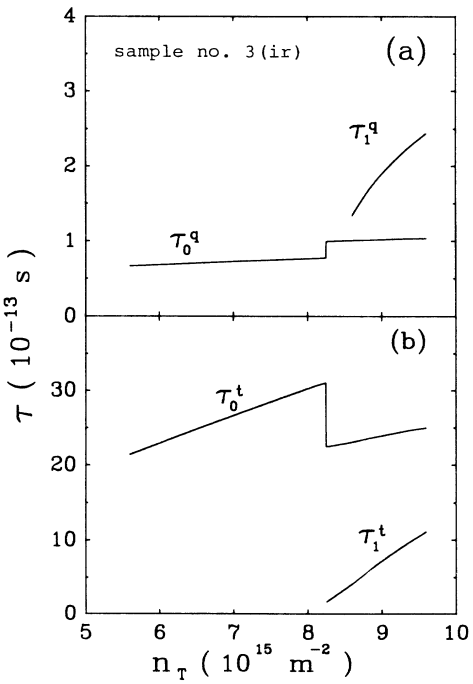


FIG. 11. The calculated transport and quantum lifetimes ($\tau^t$ and $\tau^q$) of the electrons in the two bands of sample 3 as a function of total areal density $n_T$ for ir illumination. The calculations are for $E_{dd} = 180$ meV and correspond to the mobilities shown in Fig. 10(b) for ir.

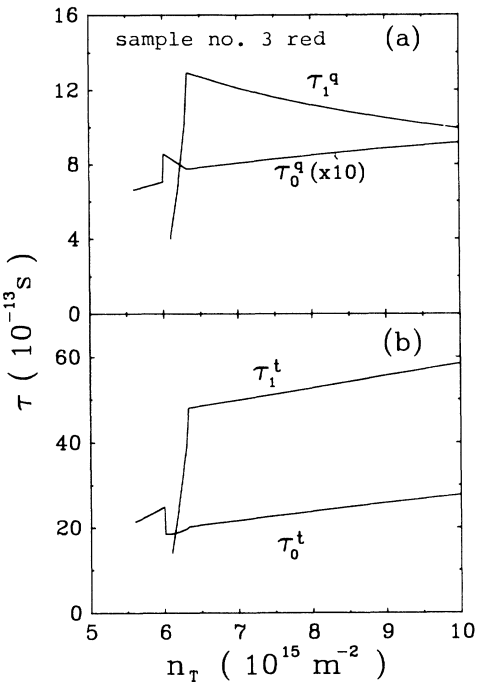


FIG. 12. As Fig. 11 but for red illumination.

subband electrons takes on the values

$$\frac{1}{\tau_0^t} = \frac{1}{\tau_{00}^t} \tag{5}$$

just below and

$$\frac{1}{\tau_0^t} = \frac{1}{\tau_{00}^t} + \frac{1}{\tau_{01}^t} \tag{6}$$

just above the second subband edge. $(\tau_{00}^t)^{-1}$ represents the intrasubband scattering rate while $(\tau_{01}^t)^{-1}$, Eq. (A35), is directly related to the rate of intersubband scattering and is partially responsible for the mobility discontinuity. (See the Appendix for further discussion of this point.) If the effect of disorder broadening were to be taken into account, the density of available final states for electrons in the lowest subband to scatter into would increase continuously and the mobility discontinuity would be broadened into a smooth transition.

In Figs. 11(a) and 12(a) we also show the quantum lifetimes $\tau^q$ for the two subbands calculated using Eq. (A36). In contrast to the transport lifetimes, these lifetimes are dominated by small angle scattering and $\tau_0^q$ is typically an order of magnitude smaller than $\tau_0^t$. It is interesting to note that $\tau_0^t > \tau_1^t$ but $\tau_0^q < \tau_1^q$ for ir illumination. These observations show that the relative magnitudes of the various lifetimes depend sensitively on the conditions of the junction and the way in which the momentum dependence of the scattering probability is sampled. As a last point, we note the different behavior of $\tau_0^t$ and $\tau_0^q$ at the onset of second-band occupancy; $\tau_0^t$ is observed to decrease, as expected, as intersubband scattering turns on, while $\tau_0^q$ is seen to *increase*. As explained previously,[14] this apparently paradoxical behavior of $\tau_0^q$ is due to the fact the second subband electrons enhance the screening of the impurity potential, thereby diminishing the scattering rate of the electrons in the first subband. This additional screening is most effective at small momentum transfers, which dominate the single particle scattering rate, but much less effective for large momentum transfers ($q \sim 2k_{F0}$) which are relevant to the conductivity.

## V. CONCLUSIONS

In this paper we have investigated persistent photoconductivity in GaAs/$Al_xGa_{1-x}As$ heterojunctions and have confirmed the dependence of the carrier generation mechanism on the nature of the incident radiation. Frequencies below the GaAs band gap lead to ionization of the *DX* centers in the Si-doped $Al_xGa_{1-x}As$ layer, while above gap radiation is an efficient source of *e-h* pairs. In the latter case, the elimination of the acceptor depletion layer in the GaAs appears as a distinct feature in the 2D EG density versus illumination curve, and allows one to obtain a direct measure of the areal depletion charge density. The electronic subband structure is particularly sensitive to this parameter. The quantitative agreement between the results of self-consistent electronic structure calculations, which make use of the measured depletion charge densities, and the observed illumination behavior, namely, the subband occupancies versus total 2D EG density, strongly supports the validity of the interpretation.

The high resolution of our data, particularly with regard to variations with total electron density, has enabled us to observe many interesting features, especially in the region where the second subband is just beginning to be occupied. The behavior of the individual subband densities as a function of total density as seen in Fig. 3 is a good example of this, as are the sharp minima in the mobility curves of Fig. 4 and the change of slope in Fig. 5. The difference in widths of the transition region in $\langle \mu \rangle$ for red and ir has a natural explanation in terms of the fore-going model, though the absolute widths are outside the scope of our theoretical treatment. We have also presented new evidence to suggest that the electrons in the tail of the upper subband are either localized or have a very low mobility. An important conclusion of this and similar previous work[1] is that systematic controlled illumination experiments can provide detailed information about the electronic subband structure and indirectly the electrostatic field distribution throughout the heterojunction.

Our attempts to theoretically reproduce the observed impurity limited mobilities show that there are still several aspects of *DX*-center ionization which are not understood. The modeling of the state of the heterojunction cooled in the dark as one in thermodynamic equilibrium with a mixture of shallow and deep donors has not been entirely successful. We require the deep donors to have an energy level which is further removed from the conduction-band edge than is commonly accepted. This might indicate deficiencies in the model, or perhaps in the

assumption of thermodynamic equilibrium.

Furthermore, if one were to accept the *DX*-center concentrations observed in the bulk to apply to the heterojunction with its known Si doping density, then the number of potentially available PPC carriers far exceeds that appearing in the 2D EG. There are, of course, other sites to which an excess of photoexcited carriers can migrate; the electrostatic condition inferred from the subband structure dictate that these occur on the $Al_xGa_{1-x}As$ side of the junction. However, our mobility studies strongly suggest that the actual number of photoionized *DX* centers is not very different from that required to populate the 2D EG because otherwise the mobility would be degraded much more severely with illumination than is actually observed.

There are also unanswered questions of how and why saturation of PPC occurs with final 2D EG densities of typically $10^{16}$ $m^{-2}$, and what final state is achieved after illumination. It is possible that the nature of *DX* centers in heterojunctions, or their behavior with respect to illumination, is different from that in the bulk.

Finally we note the rather complex variation of the various subband lifetimes with illumination (Figs. 11 and 12). The second-subband lifetimes are particularly sensitive to the conditions of the heterojunction. Calculations performed for the specific samples we have studied show that the second subband quantum lifetime is longer than that of the first subband over a wide range of conditions, and consistent with direct measurements of Dingle temperatures.[14] The relative magnitude of the first- and second-subband transport lifetimes is more variable and depends on the type of illumination used. In the case of the second subband, experiments using infrared LED's must include a filter to remove the above band-gap radiation since a small leakage of this red light can completely change the second subband lifetimes. Experiments, such as those reported here, on samples exhibiting multiple-band occupancy with PPC offer an ideal opportunity to investigate these impurity related problems. Further theoretical work on impurity-limited mobilities which addresses both transport and single-particle aspects (e.g., density of states) in a consistent fashion is clearly of interest.

## ACKNOWLEDGMENTS

This work was partially supported by grants from the Natural Sciences and Engineering Research Council (NSERC) of Canada.

## APPENDIX

In this Appendix we present details of the mobility calculation. Two steps are needed to arrive at the final results: (i) the calculation of the impurity-induced electron-scattering rates and (ii) the solution of the Boltzmann transport equation for a multiband situation. The transport problem is treated using the formalism of Siggia and Kwok.[19]

The geometry of interest is described in Sec. IV B. We assume that the mobility is limited by ionized impurity scattering which includes scattering from the remote ionized Si donors in the $Al_xGa_{1-x}As$ and from the ionized acceptors in the GaAs. Since the acceptor density in our samples is much smaller than the donor density, the donor impurities provide the dominant scattering mechanism. However, for completeness we include both mechanisms in our transport calculations.

The impurities give rise to a fluctuating potential $V(\mathbf{r})$ which induces electronic transitions between the subband states $|i\mathbf{k}\rangle$ with energy $E_{i\mathbf{k}}$. The transition rate, given by

$$w_{i\mathbf{k}\to j\mathbf{k}'}=(2\pi/\hbar)|\langle j\mathbf{k}'|V|i\mathbf{k}\rangle|^2\delta(E_{i\mathbf{k}}-E_{j\mathbf{k}'}) \tag{A1}$$

is the essential element in the Boltzmann transport theory. The transition-matrix element can be expressed as

$$\langle j\mathbf{k}'|V|i\mathbf{k}\rangle=\frac{1}{A}\int d\mathbf{r}\,\psi_j(z)e^{-i\mathbf{k}'\cdot\rho}V(\mathbf{r})\psi_i(z)e^{i\mathbf{k}\cdot\rho}$$
$$=\frac{1}{A}\int dz\,\psi_j(z)V(z;\mathbf{q})\psi_i(z)\ , \tag{A2}$$

with

$$V(z;\mathbf{q})=\int d\rho\,e^{-i\mathbf{q}\cdot\rho}V(\mathbf{r})\ . \tag{A3}$$

Here $\mathbf{q}=\mathbf{k}'-\mathbf{k}$ is the electron momentum transfer in the plane of the junction; $V(z;\mathbf{q})$ is the two-dimensional Fourier transform of $V(\mathbf{r})$, and $A$ is the area of the junction.

We consider first the contribution to $V(\mathbf{r})$ from the ionized donors which are located at the positions $\mathbf{R}_i$ to the left ($z<0$) of the interface. These positions are distributed randomly throughout the donor space-charge layer and a configuration average of the transition rate must eventually be performed. Each impurity, assumed to carry a charge $e$, gives rise to a Coulomb potential which is screened by the dielectric constant $\epsilon$. [If the dielectric constants on either side of the junction are $\epsilon_1$ and $\epsilon_2$, $\epsilon$ is the average $\frac{1}{2}(\epsilon_1+\epsilon_2)$.] The electrostatic potential of the donor impurities in cgs units is thus

$$\phi^{\rm ext}(\mathbf{r})=\sum_i\frac{e}{\epsilon|\mathbf{r}-\mathbf{R}_i|} \tag{A4}$$

and its two-dimensional Fourier transform is

$$\phi^{\rm ext}(z;\mathbf{q})=\sum_i e^{qZ_i}e^{-i\mathbf{q}\cdot\mathbf{R}_i}\frac{2\pi e}{\epsilon q}e^{-qz} \tag{A5}$$

at space points for which $z>Z_i$.

The external electrostatic potential $\phi^{\rm ext}(\mathbf{r})$ does not itself scatter the electrons since it is screened by the 2D EG. We calculate this screening in the random-phase approximation, including only the Hartree field. In principle, the density-functional exchange-correlation potential should also be included but, since it is of secondary importance, we shall follow the common practice of neglecting its effect. The scattering potential is then given by $V(\mathbf{r})=-e\phi(\mathbf{r})$, where $\phi(\mathbf{r})$ is the fluctuating part of the total electrostatic potential due to all charges in the system.

The linear screening problem is standard and we simply outline the essential steps in the derivation. It is convenient to define the transition densities

$$f_\alpha(z)=\psi_i(z)\psi_j(z)\ , \tag{A6}$$

where the index $\alpha$ denotes the pair of subband indices $(ij)$. We then have

$$\langle j\mathbf{k}'|V|i\mathbf{k}\rangle=-\frac{e}{A}\int dz\, f_\alpha(z)\phi(z;\mathbf{q})\ ,$$

$$\equiv-\frac{e}{A}\phi_\alpha(\mathbf{q})\ . \tag{A7}$$

The quantities $\phi_\alpha(\mathbf{q})$ are essentially intersubband transition matrix elements. The matrix element $\phi_\alpha^{\rm ext}(\mathbf{q})$ is similarly defined and from (A5) we have

$$\phi_\alpha^{\rm ext}(\mathbf{q})=\frac{2\pi e}{\epsilon q}\sum_i e^{qZ_i}e^{-i\mathbf{q}\cdot\mathbf{R}_i}A_\alpha(q)\ , \tag{A8}$$

where

$$A_\alpha(q)=\int dz\, e^{-qz}f_\alpha(z)\ . \tag{A9}$$

These two matrix elements are related according to linear-response theory by the equation

$$\phi_\alpha(\mathbf{q})=\sum_\beta(\epsilon^{-1})_{\alpha\beta}\phi_\beta^{\rm ext}(\bar{\mathbf{q}})\ , \tag{A10}$$

where the dielectric matrix is defined by the following expressions:

$$\epsilon_{\alpha\beta}(q)=\delta_{\alpha\beta}+\frac{2\pi e^2}{\epsilon q}F_{\alpha\beta}(q)\chi_\beta^0(q)\ , \tag{A11}$$

$$F_{\alpha\beta}(q)=\int dz\int dz' f_\alpha(z)e^{-q|z-z'|}f_\beta(z')\ , \tag{A12}$$

and

$$\chi_{ij}^0(q)=\frac{2}{A}P\sum_{\mathbf{k}}\frac{f(E_{i\mathbf{k}})-f(E_{j,\mathbf{k}+\mathbf{q}})}{E_{j,\mathbf{k}+\mathbf{q}}-E_{i\mathbf{k}}}\ . \tag{A13}$$

$f(E)$ is the Fermi-Dirac distribution function which we take to be the zero-temperature limit. $F_{\alpha\beta}(q)=F_{ij,i'j'}(q)$ is the expression for the Coulomb form factor obtained when the dielectric constant does not change across the interface.

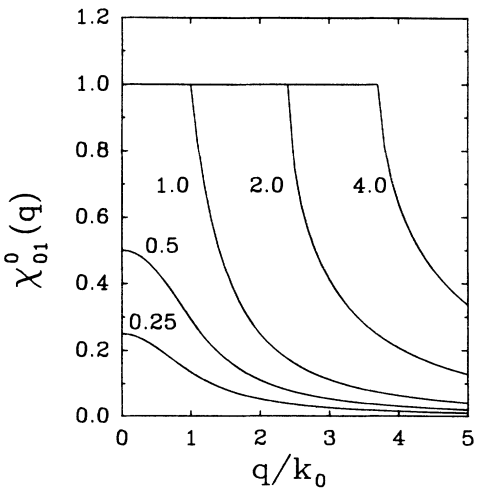


FIG. 13. Itersubband density response function for noninteracting electrons in units of $m^*/\pi\hbar^2$. The wave vector $q$ is normalized by $k_0=(2m^*E_{10}/\hbar^2)^{1/2}$ and the various curves are labeled by $E_{F0}/E_{10}$.

Equation (A13) defines the independent particle density response matrix which is symmetric in the subband indices. The diagonal terms are given by the well-known Stern result[20]

$$\chi_{ii}^0(q)=\frac{m^*}{\pi\hbar^2}\left\{1-{\rm Re}\left[1-\left[\frac{2k_{Fi}}{q}\right]^2\right]^{1/2}\right\}\Theta(E_F-E_i)\ . \tag{A14}$$

The off-diagonal elements are less familiar but have been used in other contexts.[21] Assuming that $E_i<E_j$ and defining $\hbar^2k_0^2/2m^*=E_j-E_i$, the off-diagonal terms are given by

$$\chi_{ij}^0(q)=\begin{cases}\dfrac{m^*}{\pi\hbar^2}\left[\dfrac{q^2+k_0^2}{2q^2}-\dfrac{1}{2q^2}[(q^2+k_0^2)^2-(2qk_{Fi})^2]^{1/2}\right] & \text{for } k_{Fi}<k_0\\ \dfrac{m^*}{\pi\hbar^2}\left[1-\dfrac{1}{q^2}\Theta(q-k_+)[(q^2-k_+^2)(q^2-k_-^2)]^{1/2}\right] & \text{for } k_{Fi}>k_0\ .\end{cases} \tag{A15}$$

The first form is valid when only the lower subband is occupied while the second applies when both are occupied. The critical wave vectors $k_\pm$ are defined as

$$k_\pm=|k_{Fi}\pm k_{Fj}| \tag{A16}$$

provided, of course, that both Fermi wave vectors are finite. The $q$ dependence of $\chi_{ij}^0(q)$ for various positions of the Fermi level is shown in Fig. 13.

In our calculations we have truncated the response matrix to include only the lowest two subband states, i.e., the index $\alpha$ takes on four distinct values. Reference to Fig. 13 shows that the screening provided by higher subbands can be significant even when these bands are not occupied. Truncation of the response matrix underestimates the ability of the electron gas to screen the external potential and hence overestimates the scattering rate. This point is mentioned in Sec. IV, but more work needs to be done to determine the quantitative importance of higher subbands to the screening properties of a 2D EG.

The quantity $\phi_\alpha(q)$ still depends on the positions of the impurities through Eq. (A8). Its square must, therefore, be averaged over impurity configurations. Denoting the average by a bar, we finally obtain

$$|V_{ij}^d(q)|^2\equiv\overline{A|\langle j\mathbf{k}'|V|i\mathbf{k}\rangle|^2}\ ,$$

$$=n_d f(q)\left[(2\pi e^2/\epsilon q)\sum_\beta(\epsilon^{-1})_{\alpha\beta}A_\beta\right]^2\ . \tag{A17}$$

with the donor impurity form factor

$$f(q)=\frac{1}{2qW_d}(1-e^{-2qW_d})e^{-2qs} . \tag{A18}$$

These expressions assume a single ionized impurity layer of density $n_d$, width $W_d$, and setback distance $s$. If more than one layer is present, Eq. (A17) represents the contribution from a single layer, and all such contributions must be summed. Equation (A18) shows that the transition rate for a given momentum transfer depends exponentially on the setback distance $s$. The superscript $d$ in Eq. (A17) distinguishes this result from the acceptor contribution.

A similar analysis can be carried out for the acceptor impurities although it is complicated by the fact that the impurity positions occur within the electron gas itself. Instead of (A5) we have

$$\phi^{\rm ext}(z;\mathbf{q})=-\frac{2\pi e}{\epsilon q}\sum_i e^{-i\mathbf{q}\cdot\mathbf{R}_i}e^{-q|z-Z_i|} \tag{A19}$$

and the $z$ and $Z_i$ dependences can no longer be factored. Nevertheless, the screening problem is the same and (A10) remains true. The difference arises at the configuration average stage where

$$|V_{ij}(q)|^2=\overline{A|\langle j\mathbf{k}'|V|i\mathbf{k}\rangle|^2}$$
$$=\frac{1}{A}\overline{|e\phi_\alpha(\mathbf{q})|^2}$$

with

$$\overline{|\phi_\alpha(\mathbf{q})|^2}=\sum_{\beta\gamma}(\epsilon^{-1})_{\alpha\beta}(\epsilon^{-1})_{\alpha\gamma}\overline{\phi_\beta^{\rm ext}(\mathbf{q})[\phi_\gamma^{\rm ext}(\mathbf{q})]^*}$$
$$=\left[\frac{2\pi e}{\epsilon q}\right]^2\sum_{\beta,\gamma}(\epsilon^{-1})_{\alpha\beta}(\epsilon^{-1})_{\alpha\gamma}$$
$$\times\sum_{i,j}\overline{e^{-i\mathbf{q}\cdot(\mathbf{R}_i-\mathbf{R}_j)}\int dz\,f_\beta(z)e^{-q|z-Z_i|}\int dz'f_\gamma(z')e^{-q|z'-Z_j|}} . \tag{A20}$$

In performing the configuration average of the indicated quantity, only the $i=j$ terms need be retained and we obtain

$$An_a\int dz\int dz'f_\beta(z)f_\gamma(z')\frac{1}{W_a}\int_0^{W_a}d\bar{z}\,e^{-q|z-\bar{z}|}e^{-q|z'-\bar{z}|} , \tag{A21}$$

where we have assumed the acceptor impurities of areal density $n_a$ to be confined between $z=0$ and $z=W_a$.

A lengthy but straightforward calculation yields

$$F_a(z,z',q)\equiv\frac{1}{W_a}\int_0^{W_a}d\bar{z}\,e^{-q|z-\bar{z}|}e^{-q|z'-\bar{z}|} ,$$
$$=\frac{1}{qW_a}[(1+q|z-z'|)e^{-q|z-z'|}-\tfrac{1}{2}e^{-q(z+z')}-\tfrac{1}{2}e^{-q(2W_a-z-z')}] \tag{A22}$$

for $0\le z,z'\le W_a$. $F_a$ tends to unity for $q\to 0$. For large $W_a$, the last term in $F_a$ is small for the $z,z'$ values of interest unless $q\le W_a^{-1}$. With the result Eq. (A22), Eq. (A21) becomes

$$\frac{An_a}{qW_a}\left[F_{\beta\gamma}(q)-q\frac{\partial F_{\beta\gamma}}{\partial q}-\frac{1}{2}A_\beta A_\gamma-\frac{1}{2}B_\beta B_\gamma\right] \tag{A23}$$

with $F_{\beta\gamma}$ and $A_\beta$ defined in Eqs. (A12) and (A9), respectively, and $B_\beta$ is given by

$$B_\beta(q)=\int dz\,e^{-q(W_a-z)}f_\beta(z) . \tag{A24}$$

With these results we finally obtain

$$|V_{ij}^a(q)|^2=\left[\frac{2\pi e^2}{\epsilon q}\right]^2\frac{N_a}{q}\sum_{\beta,\gamma}(\epsilon^{-1})_{\alpha\beta}(\epsilon^{-1})_{\alpha\gamma}\left[F_{\beta\gamma}-q\frac{\partial F_{\beta\gamma}}{\partial q}-\frac{1}{2}A_\beta A_\gamma-\frac{1}{2}B_\beta B_\gamma\right] . \tag{A25}$$

Since $N_a\ll N_d$, $|V_{ij}^a(q)|^2$ is small compared to $|V_{ij}^d(q)|^2$ for the samples we have studied. However, the acceptor impurities can make an important contribution in other situations as, for example, when the donor impurities are set back well away from the junction.

We turn next to the calculation of the mobility. Siggia and Kwok[19] showed that the Boltzmann transport equation for the multiband situation can be reduced to the form

$$\sum_j K_{ij}\tau_j^t=E_{Fi} \tag{A26}$$

where $E_{Fi}$ is the Fermi level of $i$th subband ($E_{Fi}=E_F-E_i$) and $\tau_i^t$ is the subband transport lifetime. The summation ex-

tends over all occupied subbands. The experimentally measurable quantity is the average mobility $\langle\mu\rangle$, which is defined as

$$\langle\mu\rangle=\frac{e}{m^* n_T}\sum_i n_i\tau_i^t \ . \tag{A27}$$

The transport scattering matrix $K_{ij}$ is given in terms of the transition-matrix elements by

$$\begin{aligned}K_{ij}&=\frac{2\pi^2\hbar^3}{m^{*2}}\int\frac{d\mathbf{k}}{(2\pi)^2}\int\frac{d\mathbf{k}'}{(2\pi)^2}\left[\delta_{ij}\sum_l|V_{il}(q)|^2\delta(E_{Fi}-\varepsilon_{\mathbf{k}})\delta(E_{Fl}-\varepsilon_{\mathbf{k}'})k^2-|V_{ij}(q)|^2\delta(E_{Fi}-\varepsilon_{\mathbf{k}})\delta(E_{Fj}-\varepsilon_{\mathbf{k}'})\mathbf{k}\cdot\mathbf{k}'\right]\\&=\delta_{ij}\sum_l K_{il}^{(1)}-K_{ij}^{(2)} \ .\end{aligned} \tag{A28}$$

This expression assumes zero temperature and a constant density of states for each subband above its subband edge. The two terms $K_{ij}^{(1)}$ and $K_{ij}^{(2)}$ can be expressed equivalently as

$$\begin{aligned}K_{ij}^{(1)}&=\frac{2\pi^2\hbar^3}{m^{*2}}\int\frac{d\mathbf{k}}{(2\pi)^2}\int\frac{d\mathbf{k}'}{(2\pi)^2}|V_{ij}(q)|^2\delta(E_{Fi}-\varepsilon_{\mathbf{k}})\delta(E_{Fj}-\varepsilon_{\mathbf{k}'})k^2 \ ,\\&=\frac{k_{Fi}^2}{\pi\hbar}\int_{k_-}^{k_+}dq\frac{q|V_{ij}(q)|^2}{[(k_+^2-q^2)(q^2-k_-^2)]^{1/2}} \ ,\\&=\frac{k_{Fi}^2}{2\pi\hbar}\int_0^{\pi}d\theta|V_{ij}(q_{ij})|^2, \quad q_{ij}=[k_{Fi}^2+k_{Fj}^2-2k_{Fi}k_{Fj}\cos\theta]^{1/2} \ ,\end{aligned} \tag{A29}$$

and

$$\begin{aligned}K_{ij}^{(2)}&=\frac{2\pi^2\hbar^3}{m^{*2}}\int\frac{d\mathbf{k}}{(2\pi)^2}\int\frac{d\mathbf{k}'}{(2\pi)^2}|V_{ij}(\mathbf{q})|^2\delta(E_{Fi}-\varepsilon_{\mathbf{k}})\delta(E_{Fj}-\varepsilon_{\mathbf{k}'})\mathbf{k}\cdot\mathbf{k}' \ ,\\&=\frac{1}{2\pi\hbar}\int_{k_-}^{k_+}dq\frac{q(k_{Fi}^2+k_{Fj}^2-q^2)}{[(k_+^2-q^2)(q^2-k_-^2)]^{1/2}}|V_{ij}(q_{ij})|^2 \ ,\\&=\frac{k_{Fi}k_{Fj}}{2\pi\hbar}\int_0^{\pi}d\theta\cos\theta|V_{ij}(q_{ij})|^2 \ .\end{aligned} \tag{A30}$$

The limiting wave vectors $k_\pm$ were defined in Eq. (A16). $K_{ij}^{(2)}$ is a symmetric matrix but $K_{ij}^{(1)}$ is not.

For a single occupied band ($i=0$) we find from Eqs. (A26), (A29), and (A30) the expected result

$$\frac{1}{\tau_0^t}=\frac{K_{00}}{E_{F0}}=\frac{m^*}{\pi\hbar^3}\int_0^{\pi}d\theta(1-\cos\theta)|V_{00}(q)|^2 \tag{A31}$$

with $q=2k_{F0}\sin(\theta/2)$. It should be noted however that even in this situation the existence of higher subbands makes itself felt through their effect on the screening of the impurity potential, i.e., the calculation of $|V_{00}(q)|^2$ is still a multiband problem [see Eq. (A17)]. In our work we take into account only the two lowest subbands. Equation (A31) reduces to the result of Lee *et al.*[28] with the following further approximations: (i) neglect of excited subband polarization, (ii) neglect of the $q$ dependence of the Coulomb form factor, (iii) the replacement of $A_0(q)$ by $e^{-q\langle z\rangle_0}$ where $\langle z\rangle_0$ is the average extent of the first subband wave function. These approximations were not made in our numerical calculations.

The solution of (A26) for the two-subband model yields

$$\frac{1}{\tau_0^t}=\frac{K_{00}K_{11}-K_{01}K_{10}}{E_{F0}K_{11}-E_{F1}K_{01}} \ , \tag{A32}$$

$$\frac{1}{\tau_1^t}=\frac{K_{00}K_{11}-K_{01}K_{10}}{E_{F1}K_{00}-E_{F0}K_{10}} \ . \tag{A33}$$

These general expressions are difficult to interpret as they are complicated mixtures of intrasubband and intersubband scattering processes. However, one interesting limit is $k_{F1}\to 0^+$, at which point intersubband scattering for the first subband turns on. In this limit,

$$\frac{1}{\tau_0^t}=\frac{1}{\tau_{00}^t}+\frac{1}{\tau_{01}^t} \ , \tag{A34}$$

where $\tau_{00}^t$ is the intrasubband lifetime given by Eq. (A31) and $\tau_{01}^t$ is the intersubband lifetime given by

$$\frac{1}{\tau_{01}}=\frac{m^*}{\hbar^3}|V_{01}(k_{F0})|^2 \ . \tag{A35}$$

This term does not arise when the second subband is unoccupied, however it should be noted that the discontinuity in the mobility is only partly due to it. Screening as determined by the dielectric matrix (A11) is also discontinuous at second subband occupancy and results in a discontinuous scattering matrix element. All of this behavior is a consequence of the assumed discontinuity in

the 2D density of states. In a more realistic description using an impurity broadened density of states, the effect of intersubband scattering on the mobility is expected to set in continuously.

Finally we give the expressions used to calculate the quantum lifetimes. These are obtained by considering the total scattering rate of a subband electron at the Fermi energy and are given by

$$\frac{1}{\tau_i^q} = \frac{m^*}{\pi\hbar^3} \sum_j \int_0^\pi d\theta |V_{ij}(q_{ij})|^2 . \quad \text{(A36)}$$


[1]J. J. Harris, D. E. Lacklison, C. T. Foxon, F. M. Selten, A. M. Suckling. R. J. Nicholas, and K. W. Barnham, Semicond. Sci. Technol. **2**, 783 (1987).

[2]C. E. Falt, C. M. Hurd, S. P. McAlister, W. R. McKinnon, D. J. Day, and A. J. Springthorpe, Semicond. Sci. Technol. **2**, 513 (1987).

[3]D. E. Lacklison, J. J. Harris, C. T. Foxon, J. Hewett, D. Hilton, and C. Roberts, Semicond. Sci. Technol. **3**, 633 (1988).

[4]A. Kastalsky and J. C. M. Hwang, Solid State Commun. **51**, 317 (1984).

[5]N. Chand, T. Henderson, J. Klem, W. T. Masselink, R. Fischer, Y.-C. Chang, and H. Morkoç, Phys. Rev. B **30**, 4481 (1984).

[6]M. O. Watanabe, K. Morizuka, M. Mashita, Y. Ashizawa, and Y. Zohta, Jpn. J. Appl. Phys. Pt. 2 **23**, L103 (1984).

[7]E. F. Schubert and K. Ploog, Phys. Rev. B **30**, 7021 (1984).

[8]E. F. Schubert, J. Knecht, and K. Ploog, J. Phys. C **18**, L215 (1985).

[9]M. Mizuta and K. Mori, Phys. Rev. B **37**, 1043 (1988).

[10]J. E. Dmochowski, J. M. Langer, and J. Raczynska, Phys. Rev. B **38**, 3276 (1988).

[11]D. J. Chadi and K. J. Chang, Phys. Rev. Lett. **61**, 873 (1988).

[12]T. Ando, J. Phys. Soc. Jpn. **51**, 3893 (1982).

[13]F. Stern and S. Das Sarma, Phys. Rev. B **30**, 840 (1984).

[14]R. Fletcher, E. Zaremba, M. D'Iorio, C. T. Foxon, and J. J. Harris, Phys. Rev. B **38**, 7866 (1988).

[15]A. H. Wison, *Theory of Metals,* 2nd ed. (Cambridge University Press, Cambridge, England, 1953).

[16]D. J. Wolford, T. F. Kuech, T. W. Steiner, J. A. Bradley, M. A. Gell, D. Ninno, and M. Jaros, Superlatt. Microstruct. **4**, 525 (1988).

[17]See, for example, J. J. Harris, C. T. Foxon, D. E. Lacklison, and K. W. J. Barnham, Superlatt. Microstruct **2**, 563 (1986).

[18]R. Piotrzkowski, J. L. Robert, E. Litwin-Staszewska, and J. P. Andre, Phys. Rev. B **37**, 1031 (1988).

[19]E. D. Siggia and P. C. Kwok, Phys. Rev. B **2**, 1024 (1970).

[20]F. Stern, Phys. Rev. Lett. **18**, 542 (1967).

[21]J. K. Jain and S. Das Sarma, Phys. Rev. B **36**, 5949 (1987).

[22]F. F. Fang, T. P. Smith III, and S. L. Wright, Surf. Sci. **196**, 310 (1988).

[23]T. P. Smith III and F. F. Fang, Phys. Rev. B **37**, 4303 (1988).

[24]H. van Houten, J. G. Williamson, M. E. I. Broekaart, C. T. Foxon, and J. J. Harris, Phys. Rev. B **37**, 2756 (1988).

[25]T. P. Smith III, F. F. Fang, U. Meirav, and M. Heiblum, Phys. Rev. B **38**, 12 744 (1988).

[26]J. J. Harris, J. M. Lagemaat, S. J. Battersby, C. M. Hellon, C. T. Foxon, and D. E. Lacklison, Semicond. Sci. Technol. **3**, 773 (1988).

[27]J. J. Harris, Acta Electron. **28**, 39 (1988).

[28]K. Lee, M. S. Shur, T. J. Drummond, and H. Morkoç, J. Appl. Phys. **54**, 6432 (1983).